Applied Composite Materials (2021) 28:321–339
https://doi.org/10.1007/s10443-021-09872-4

Sintering Temperature and Interphase Effects on Mechanical Properties of an Oxide Fiber-Reinforced Al_2O_3-SiO_2 Composite Fabricated by Sol–Gel Method

Yi Wang[1] · Ao Zhang[1] · Guang-de Li[1] · Shao-peng Liu[1] · Yang Xiang[2] · Hai-feng Cheng[2]

Received: 12 July 2020 / Accepted: 20 January 2021 / Published online: 28 January 2021

Abstract
Three-dimensional Nextel™ 440 fiber-reinforced Al_2O_3-SiO_2 matrix (N440/Al_2O_3-SiO_2) composites were fabricated by sol–gel method with sintering temperature from 1100 °C to 1400 °C. The interface engineering of the composites was carried out by employing PyC and FC interphase. The microstructure and mechanical properties of the composites were investigated. Results showed that the sintering temperature had remarkable effects on the mechanical properties of the composites. The average flexural strength of the composite without interphase decreased as the temperature increased, with fracture behaviour changing from ductile to brittle, and the highest flexural strength of 90.0 MPa was obtained for the composite fabricated at 1100 °C. However, the flexural strength of the composite with PyC interphase increased initially and then decreased, with fracture behaviour remaining ductile, and the highest flexural strength of 116.3 MPa was obtained for the composite fabricated at 1300 °C. Moreover, PyC and FC interphase could effectively weaken the interfacial bond strength and efficiently promote load transfer, thus improving the strength. For the composite fabricated at 1300 °C, the average flexural strength significantly increased after introducing the optimised PyC and FC interphase.

Keywords Sol–gel processes · Composites · Interfaces · Electron microscopy · Mechanical properties

1 Introduction

Due to low density, high damage and temperature tolerance, continuous fiber-reinforced ceramic matrix composites (CFRCMCs) are considered to be the prospective candidate materials for thermo-structural and functional applications such as aircraft engines and ultra-high-velocity

✉ Yi Wang
wycfcnudt@163.com

[1] Science and Technology On Ballistic Missile Penetration Laboratory, Beijing 100076, China

[2] Science and Technology On Advanced Ceramic Fibers and Composites Laboratory, National University of Defense Technology, Changsha 410073, China

weapons [1–3]. This is especially the case for oxide/oxide CMCs, owing to their improved damage tolerance than monolithic ceramics, thermal stability than metals and oxidation inhibition than non-oxide CMCs in extreme environments [4–6].

In the past two decades, considerable efforts have been made to investigate oxide/oxide CMCs, especially the preparation, properties and structural evolution during thermal exposure of oxide fibers [7, 8], and processsing, serving properties, failure mechanism and performance improvement of the composites [9–11]. The application of oxide/oxide CMCs is largely limited by their complex fabrication process, low damage tolerance and short service life as raw materials (e.g. oxide fibers and matrices). Relevant research work has been focused on these issues in recent years [12, 13]. Like most CFRCMCs, the mechanical behaviour of oxide/oxide CMCs is greatly determined by the fiber/matrix interface. In a tough composite, the interfacial bond strength should be appropriate not only for the load transfer from the matrix to the fiber, but also for the crack deflection, interface debonding and subsequent fiber pullout [14].

According to Prof. Zok, the interface engineering of oxide/oxide CMCs can be achieved either by porous matrix, fiber coatings or fugitive coatings, all of which promote fiber toughening, causing high in situ fiber strength and energy consumption during interface debonding, fiber bridging and pullout [15]. Owing to the advantages of high fabrication efficiency, improved strength and toughness, and long service life, porous matrix has been widely employed in oxide/oxide CMCs to provide toughening mechanisms [16, 17], and present commercially available composites mainly rely on porous alumina and mullite. Despite this, porous matrix composites are primarily manufactured from winding with 1D-filament or hot-pressing with 2D-fabric reinforcements, which cannot meet the increasing demand for complex components [12, 18]. Fiber preform could allow for the production of more complex geometries and the difficulty of crack deflection could be solved by introducing fiber coatings or fugitive coatings. Several non-oxide ceramics including BN, PyC, SiC and Si_3N_4 and oxide ceramics including ZrO_2, ZnO_2 and mixed metal oxides (MXO_4) have been thoroughly explored as interphase materials in oxide/oxide CMCs, and remarkable strength improvement was achieved [19, 20]. In our previous work, the processing, microstructure and performance of oxide/oxide CMCs were studied by employing BN and fugitive carbon (FC) interphase [21–23]. However, the combined effects of sintering temperature and PyC or FC interphase, and their effects on the mechanical properties of the composites remain to be fully elucidated.

In this study, 3D Nextel™ 440 fiber-reinforced alumina and silica matrix (N440/Al_2O_3-SiO_2) composites were fabricated by sol–gel method with varying sintering temperatures, and the interface engineering of the composites was conducted by using PyC and FC coatings. The microstructure, mechanical properties and interfacial characteristics of the composites were investigated via the combination of three-point bending test, scanning electron microscopy and transmission electron microscopy. The effects of the sintering temperature and interphase on the microstructure and strength of the composites were studied, by considering the interface characteristics and the crack propagation mode.

2 Experimental

2.1 Materials

The reinforcement was Nextel^{TM}440 fiber fabrics (BF-20, 3 M Co., USA) and the fiber strength retention after exposing 100 h at 1200 °C and 1300 °C was about 60.0% and 49.0%, respectively [24]. The use of Nextel 440 fiber was mainly based on two considerations: one

was the appropriate application temperature of the resultant composite (< 1200 °C), and the other was about low cost. Three-dimensional orthogonal preforms with the fiber volume fraction of about 40.0% were accomplished by Z-stitching ten layer fabrics at 2.5 × 2.5 needle/cm^2 with the same fiber yarn. The preforms were desized in air at 600 °C for 2 h before using. The matrix precursor was diphasic Al_2O_3-SiO_2 sol prepared from commercial boehmite and silica sols in proportion corresponding to mullite composition ($3Al_2O_3 \cdot 2SiO_2$). After calcined at 1200 °C, the ceramic yield was approximately 19.6 wt.%, and the product was composed of (δ, θ)-Al_2O_3 and amorphous SiO_2, which reacted with each other to form orthorhombic mullite above 1200 °C.

For interface engineering, the preforms were pre-coated with PyC by CVD technique employing C_3H_6–Ar system at 1000 °C with a total pressure of 1.5 kPa. The thickness of PyC coatings was controlled by varying deposition time, and the resulting thickness, determined by ten times microscope-measurement at different locations, was about 10 nm, 70 nm and 150 nm after depositing 1 h, 3 h and 5 h, respectively.

3 Preparation of the Composites

Three-dimensional N440/Al_2O_3-SiO_2 composites were fabricated by sol–gel method, including follow steps: (1) vacuum infiltrating the preform with Al_2O_3-SiO_2 sol for 6 h, (2) hot gelating the preform at 80 °C for 10 h, (3) heat treating the green body at elevated temperature for 1 h in argon atmosphere. Twelve sol–gel cycles were carried out to obtain the ultimate composites.

For the composite without interphase, uncoated preform was employed, and the heat-treatment temperature was chosen as 1100 °C, 1200 °C and 1300 °C. For interface engineering of the composites, PyC coated preform was employed, and the heat-treatment temperature was chosen as 1200 °C, 1300 °C and 1400 °C. The composite with FC interphase was obtained by oxidizing the composite with PyC interphase fabricated at 1300 °C in air at 600 °C for 2 h.

4 Characterization

Density and porosity of the composites were measured by Archimedes principle. Flexural strength and modulus were characterized by room-temperature three-point bending (TPB) test on INSTRON 1342, with the sample dimension of 60 mm × 5 mm × 4 mm. The support span and loading speed was set as 50 mm and 0.5 mm/min, respectively. The average value was calculated through five samples. Elastic modulus of the matrix in the composites was studied by Nano-indentation on MTS Nanoindenter XP equipped with a Berkovich diamond indenter. More than 10 indents were carried out at a maximum load of 10 mN and the Oliver-Pharr method was employed for calculation [25]. Toughness of the matrix was calculated from work of fracture using chevron-notched specimens with the same dimensions [17].

Microstructure analysis of the composites was carried out by SEM on Hitachi S-4800. Interfacial characteristics of the composites were analyzed by TEM on Tecnai F20, with the specimen processed by FIB technique on Helios nanolab 600i.

5 Results and Discussion

5.1 Characteristics of the Composite without Interphase

Figure 1 shows cross-section morphology of N440/Al_2O_3-SiO_2 composite without interphase fabricated at different temperatures. A large number of micropores were ditributed in the composite, both inside and outside of fiber bundles, and few cracks could be observed. As the sintering temperature was increased, the number and size of micropores gradually decreased, especially for those located inside the fiber bundles.

Properties of N440/Al_2O_3-SiO_2 composite without interphase are listed in Table 1. As the sintering temperature increased from 1100 °C to 1300 °C, the density increased from 1.92 g/

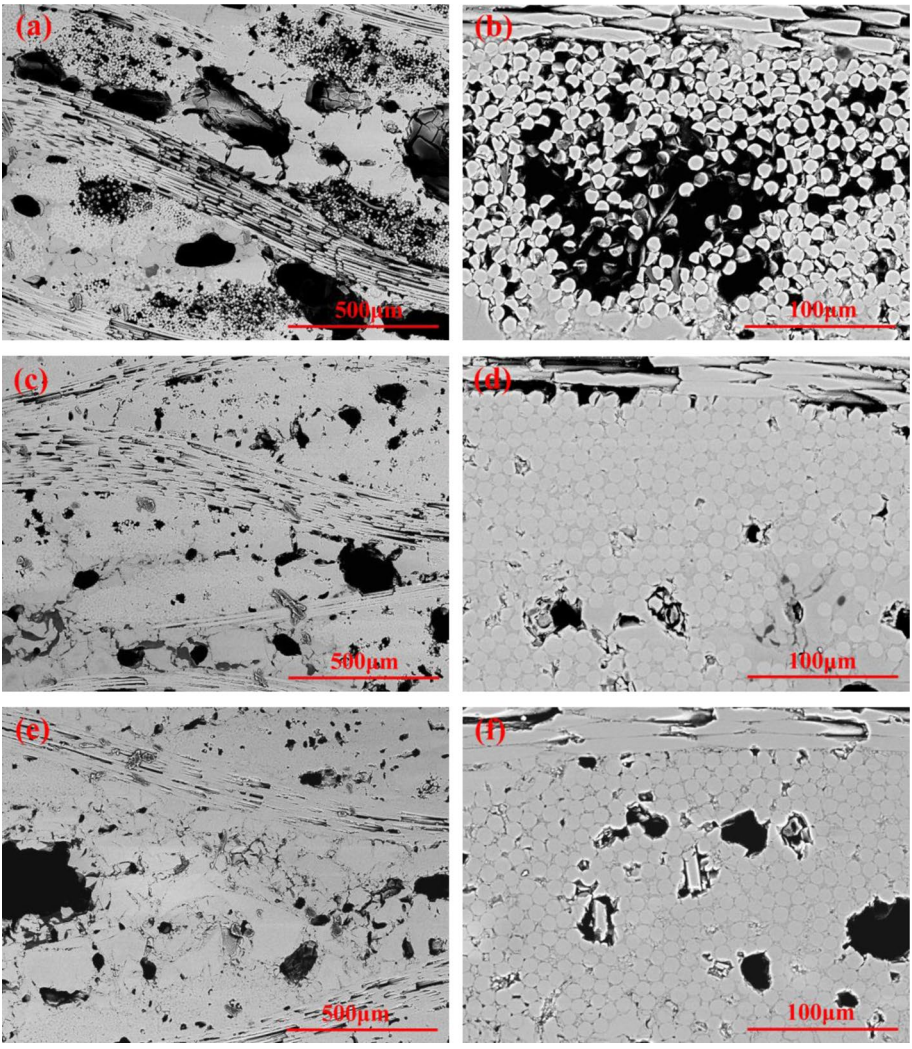

Fig. 1 Cross-section morphology of the composite without interphase fabricated at different temperatures: (**a**)(**b**) 1100 °C, (**c**)(**d**) 1200 °C and (**e**)(**f**) 1300 °C

Table 1 Properties of N440/Al_2O_3-SiO_2 composite with different fabrication parameter

Sintering temperature (°C)	Interphase	Density ($g \cdot cm^{-3}$)	Open porosity (%)	Total porosity (%)	Flexural strength (MPa)	Elastic modulus (GPa)
1100	None	1.92	12.5	35.1	90.0 ± 6.8	35.0 ± 0.7
1200	None	2.08	9.2	30.7	54.0 ± 1.8	40.8 ± 0.4
1300	None	2.38	6.4	18.6	56.7 ± 2.8	63.7 ± 1.9
1200	PyC, 10 nm	2.08	9.0	30.7	89.0 ± 5.0	31.4 ± 1.5
1200	PyC, 70 nm	2.01	9.8	33.0	77.0 ± 9.5	25.2 ± 4.6
1200	PyC, 150 nm	2.00	10.1	33.4	73.8 ± 6.0	26.2 ± 1.5
1300	PyC, 10 nm	2.34	6.9	20.0	81.9 ± 2.0	45.6 ± 1.6
1300	PyC, 70 nm	2.28	7.5	22.0	107.7 ± 2.7	40.2 ± 1.4
1300	PyC, 150 nm	2.28	7.5	22.0	116.3 ± 6.6	37.6 ± 3.5
1400	PyC, 10 nm	2.32	5.5	20.7	73.8 ± 7.6	64.3 ± 1.5
1400	PyC, 70 nm	2.30	6.0	21.4	79.7 ± 2.5	43.0 ± 1.1
1300	FC, 10 nm	2.32	7.5	20.7	78.6 ± 1.8	32.7 ± 2.8
1300	FC, 70 nm	2.26	8.1	22.7	100.9 ± 7.2	30.0 ± 1.4
1300	FC, 150 nm	2.25	8.1	22.9	95.6 ± 6.0	22.2 ± 0.2

cm^3 to 2.38 g/cm^3, and the total porosity decreased from 35.1% to 18.6% due to the densification of the matrix. Moreover, the average flexural strength decreased from 90.0 MPa to 56.7 MPa due to the decreased matrix porosity, improved interfacial bond strength and decreased in situ fiber strength. Conversely, the elastic modulus increased from 35.0 GPa to 63.7 GPa due to the densification and mullitization of the matrix. Typical flexural load–displacement curves are plotted in Fig. 2. As shown in the figure, the composite fabricated at 1100 °C displayed typical ductile fracture behaviour with the maximum integrated area under the curve, whereas the one fabricated at 1300 °C showed typical brittle fracture behaviour with the minimum integrated area. The lowest average flexural strength of 54.0 MPa was obtained for the composite fabricated at 1200 °C. The fracture behaviour difference should be attributed to the interfacial characteristic

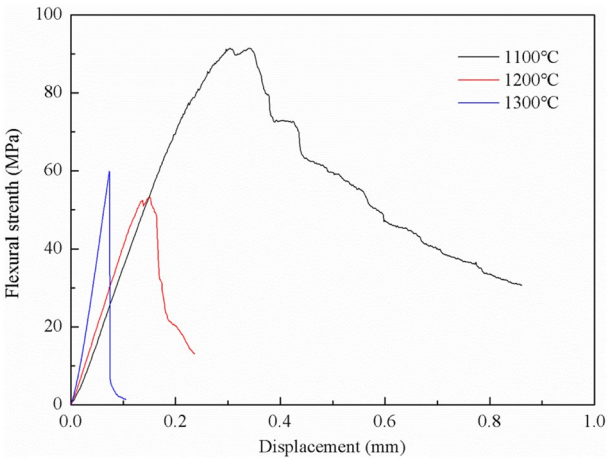

Fig. 2 Typical flexural load–displacement curves of the composite without interphase

difference induced by sintering temperature [26]. Weak interfacial bond strength, which favours ductile fracture behaviour, was obtained at low sintering temperature, whereas interfacial bond was strengthened with increasing temperature, thus leading to brittle fracture behaviour. Owing to higher mullitization and densification degree, the composite fabricated at 1300 °C had slightly higher flexural strength compared with the one fabricated at 1200 °C.

Fracture surface of the composite without interphase fabricated at different temperature after the TPB test is illustrated in Fig. 3. For the composite fabricated at 1100 °C (Fig. 3a, b), long fiber pullout behaviour could be observed at the fracture surface. As shown in Fig. 4a, a large number of matrices adhered to the pullout fiber and cracks could effectively deflect at the fiber/matrix interface. The pullout behaviour mainly originated from the weak interfacial bonding induced by the weak interfacial interaction and high matrix porosity, allowing interface

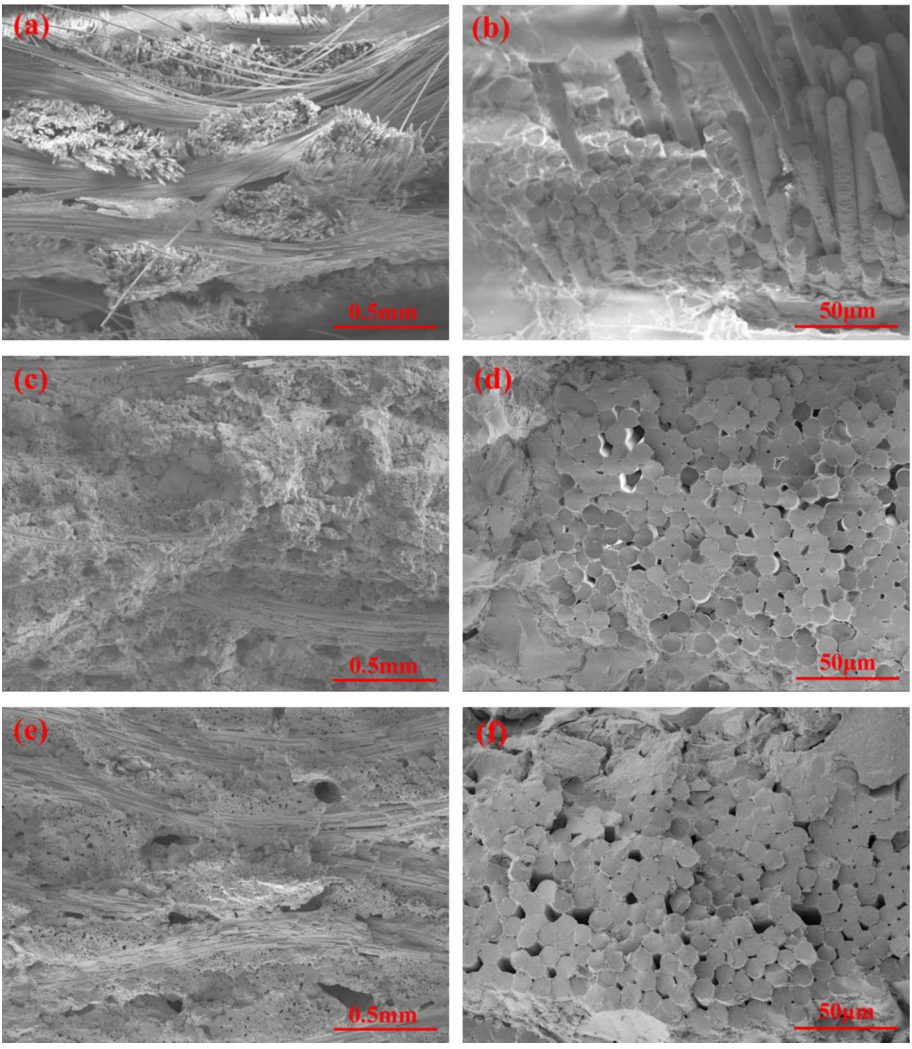

Fig. 3 Fracture surface of the composite without interphase fabricated at different temperatures: (**a**)(**b**) 1100 °C, (**c**)(**d**) 1200 °C and (**e**)(**f**) 1300 °C

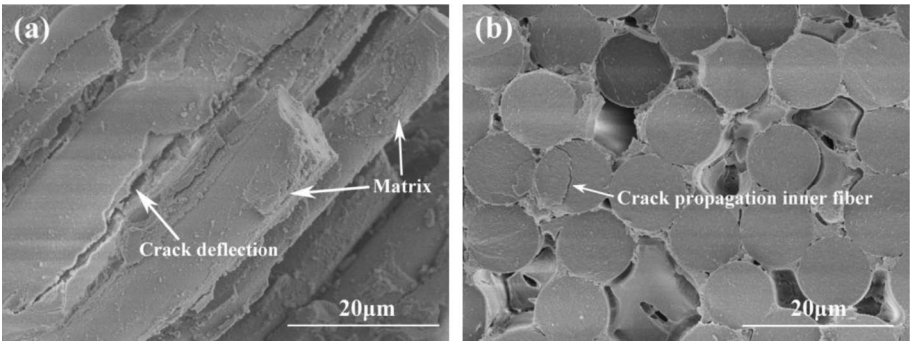

Fig. 4 (**a**) surface morphology of the pullout fiber in the composite without interphase fabricated at 1100 °C, and (**b**) matrix crack propagation behaviour inner fiber in the composite fabricated at 1200 °C

debonding to easily occur. In comparison, the composite fabricated at 1200 °C and 1300 °C showed a much flat fracture surface with no fiber pullout (Fig. 3c-f), owing to the strong interfacial bonding resulting from the strong interfacial interaction and low matrix porosity at these temperatures. As shown in Fig. 4b, the crack penetration from the matrix into the fiber confirmed the strong interfacial bonding in the composite fabricated at high temperature.

The fiber/matrix interface in the composite without interphase fabricated at 1200 °C was characterized by TEM. Figure 5 shows that extensive grains were distributed in the inner fiber and matrix, and a fuzzy interface was obtained. Moreover, a mullite grain that originated from

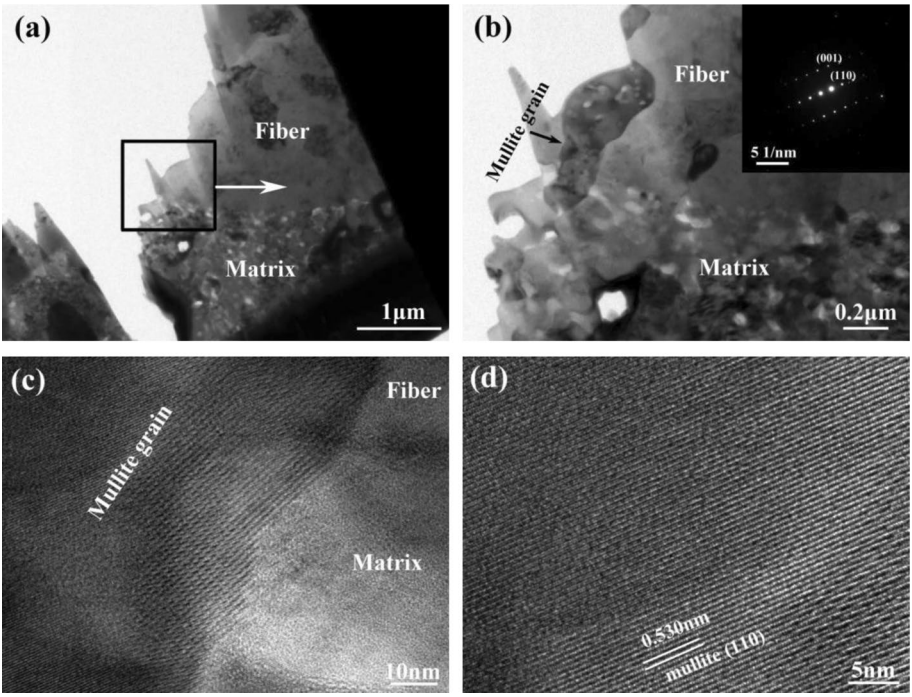

Fig. 5 TEM analysis of the fiber/matrix interface in the composite without interphase fabricated at 1200 °C

interfacial interaction existed at the interface, which confirmed that the temperature induced interfacial bond strengthening.

6 Characteristics of the Composite with PyC Interphase

Figure 6 shows cross-section morphology of N440/Al_2O_3-SiO_2 composite with different thickness of PyC interphase fabricated at 1300 °C. For all composites, the densification degree was high without few micropores, and the contour profile of the fiber was very clear. As shown in high-magnification images (Fig. 6b, d and f), a thin PyC layer with close

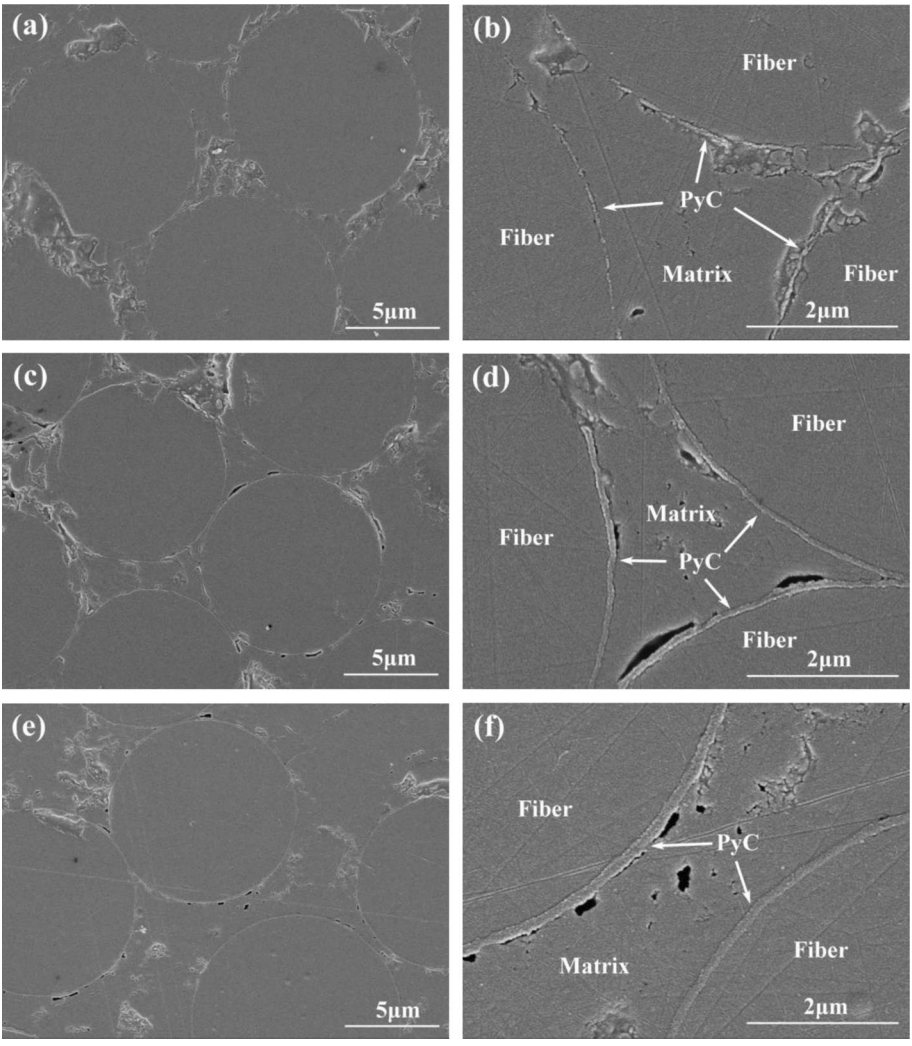

Fig. 6 Cross-section morphology of the composite with different thickness of PyC interphase fabricated at 1300 °C: (**a**)(**b**) 10 nm, (**c**)(**d**) 70 nm and (**e**)(**f**) 150 nm

structure and uniform thickness was present between the fiber and matrix. The boundary amongst the fiber, interphase and matrix was very distinct, indicating not only the stability of PyC coatings during the sol–gel process but good physical and chemical compatibility of these constituents.

As shown in Table 1, compared with the corresponding composite without interphase, the density of the composite with PyC interphase decreased, whereas the total porosity slightly increased, which can be attributed to the blocking effect of PyC coatings on the sol impregnation process and the lower density of PyC coatings than the Al_2O_3-SiO_2 matrix. In general, the density of the composite with PyC interphase increased as the sintering temperature increased but decreased gradually as the thickness of the PyC interphase increased. The opposite trend was observed for the porosity, and the same trend was noted for the elastic modulus. As the thickness of the PyC interphase increased, the average flexural strength of the composite fabricated at 1200 °C decreased from 89.0 MPa to 73.8 MPa, with the elastic modulus decreasing from 31.4 GPa to 26.2 GPa, and the average flexural strength of the composite fabricated at 1300 °C increased from 81.9 MPa to 116.3 MPa, with the elastic modulus decreasing from 45.6 GPa to 37.6 GPa. The highest value of 116.3 MPa was obtained for the composite fabricated at 1300 °C because of higher mullitization and densification degree than the one fabricated at 1200 °C but lower fiber thermal -degradation degree than the one fabricated at 1400 °C. Figure 7 shows that the composite with the PyC interphase displayed ductile fracture behaviour. For the composite fabricated at 1200 °C, the typical flexural load–displacement curve illustrated a plateau

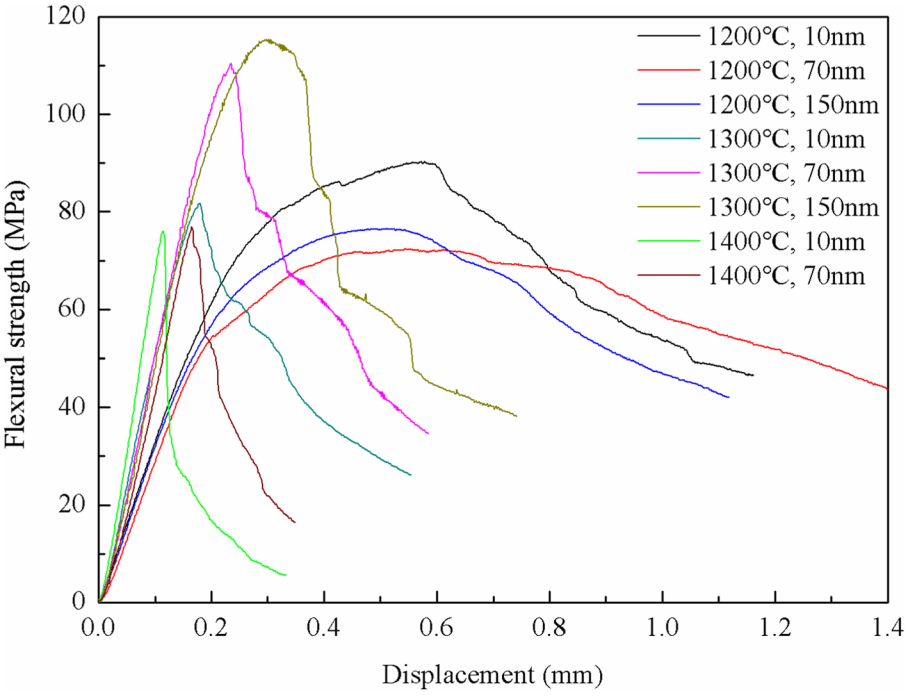

Fig. 7 Typical flexural load–displacement curves of the composite with different thickness of PyC interphase fabricated at different temperatures

after the load reached the maximum, indicating unideal fiber toughening effect originating from relatively weak interfacial bonding [27]. However, for the composite fabricated at 1400 °C, the load decreased rapidly after reaching the maximum, and the integral area under the curve was small, indicating unideal fiber toughening effect originating from low in situ fiber strength due to exposure at high sintering temperature [28]. Moreover, for the composite fabricated at 1300 °C, the curve showed a standard ductile fracture behaviour. The load decreased gradually after reaching the maximum without any plateau, and the integral area under the curve was large, indicating ideal fiber toughening effect originating from relatively suitable in situ fiber strength and interfacial bond strength.

Figure 8 shows that the composite with different thickness of PyC interphase fabricated at different temperatures displayed typical fiber pullout behaviour. The length of pullout fiber decreased gradually as the sintering temperature increased but increased as the thickness of the PyC interphase increased for the composite fabricated at 1300 °C. As shown in Fig. 8a and b, the longest length of the pullout fiber and the loosest matrix inner fiber bundle were observed at the fracture surface of the composite with 10 nm PyC interphase fabricated at 1200 °C, which implied an inefficient load transfer from the matrix to the fiber. However, for the composite with a 70 nm-thick PyC interphase fabricated at 1400 °C (Fig. 8g, h), the shortest length of the pullout fiber and the densest matrix inner fiber bundle were observed because of the lowest in situ fiber strength and the highest densification degree. For the composite with a 70 nm-thick PyC interphase fabricated at 1300 °C (Fig. 8c–f), the length of the pullout fiber and the density of the matrix inner fiber bundle were suitable, owing to appropriate in situ fiber strength and interfacial bond strength. High-magnification image (Fig. 9) shows that cracks could propagate efficiently from the matrix to the fiber, and fiber toughening mechanisms including debonding and pullout occurred. The PyC interphase could be found adhering to the debonding fiber and matrix, and internal split of PyC interphase occurred, which inferred that the crack could deflect either between the matrix, PyC, fiber or inner PyC.

The fiber/matrix interface in the composite with 70 nm PyC interphase fabricated at 1300 °C was analysed by TEM. As shown in Fig. 10a and b, nano grains were uniformly distributed in the fiber and matrix, and these two components were separated by a 60 nm-thick uniform inert PyC interphase without any interfacial diffusion and reaction. Concave and convex surface originating from defects and grain growth was obtained at the fiber surface. High-resolution TEM image (Fig. 10c) confirmed that the interphase was turbostratic carbon with obvious orientation, which was beneficial for crack deflection [29]. Element mapping analysis (Fig. 10d) further confirmed that a 60 nm-thick PyC interphase existed between the fiber and the matrix.

7 Characteristics of the Composite With FC Interphase

Owing to the high sintering temperature and superior strength, N440/Al_2O_3-SiO_2 composite with different thickness of PyC interphase fabricated at 1300 °C was further oxidised to obtain composite with different width of FC interphase. Here, we assumed that the width of the FC interphase was the same as the thickness of the PyC interphase. As shown in Fig. 11, the gap with uniform width originating from the oxidation of the PyC interphase was observed between the fiber and the matrix, and the gap width was consistent with the thickness of the original PyC interphase.

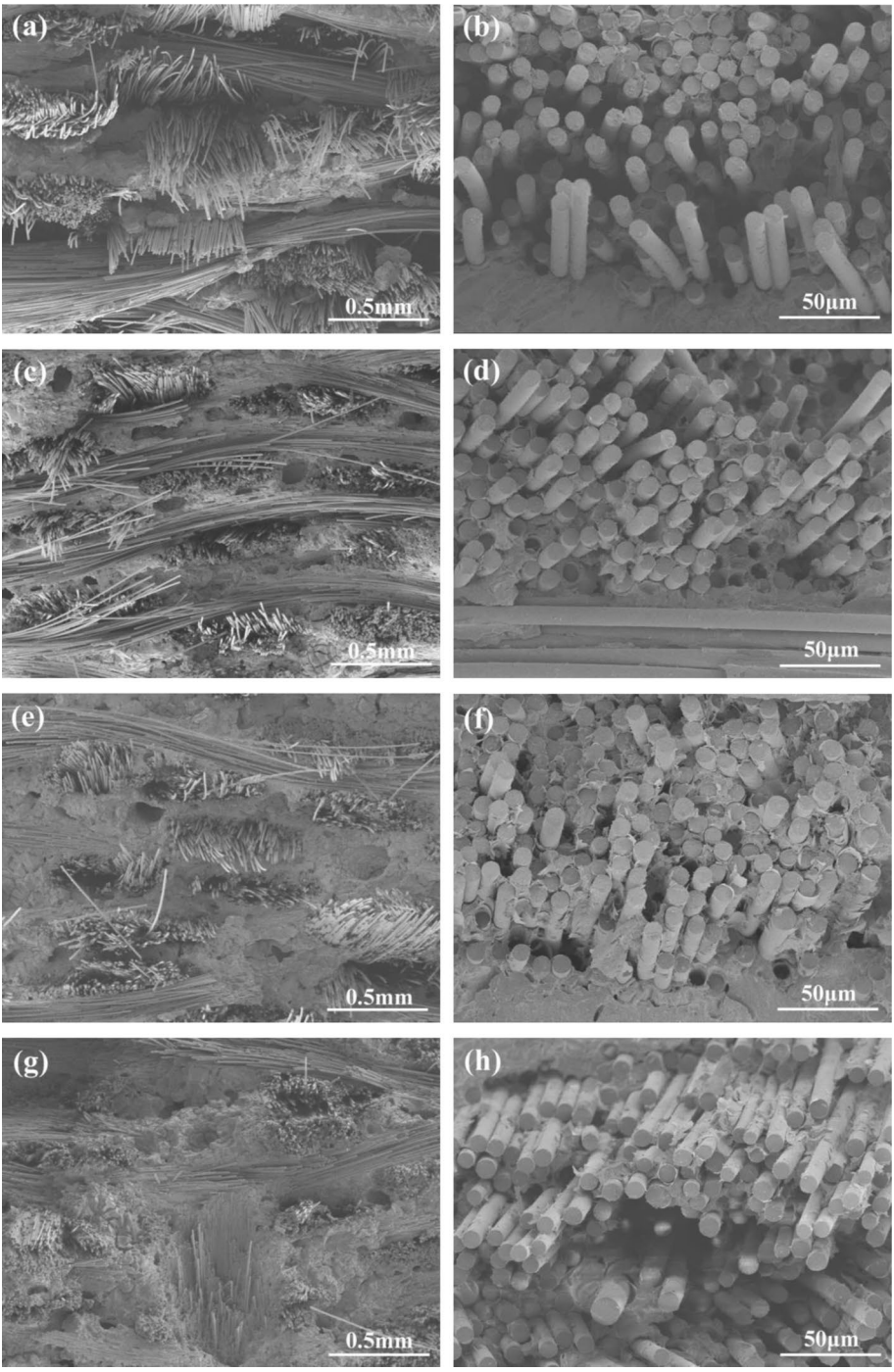

Fig. 8 Fracture surface of the composite with different thickness of PyC interphase fabricated at different temperatures: (**a**)(**b**) 1200 °C, 10 nm, (**c**)(**d**) 1300 °C, 10 nm, (**e**)(**f**) 1300 °C, 70 nm and (**g**)(**h**) 1400 °C, 70 nm

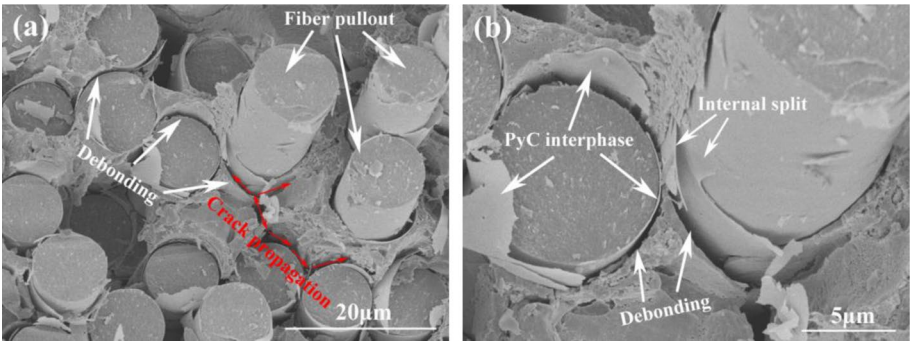

Fig. 9 Microstructure of the fiber/matrix interface in the composite with a 70 nm-thick PyC interphase fabricated at 1300 °C

As shown in Table 1, compared with the corresponding composite with PyC interphase, the density of the composite decreased, whereas the total porosity slightly increased after the oxidation of the PyC interphase. The density decreased from 2.32 g/cm^3 to 2.25 g/cm^3, whereas the total porosity increased from 20.7% to 22.9% as the gap width increased from 10 to 150 nm. The average flexural strength of the composite

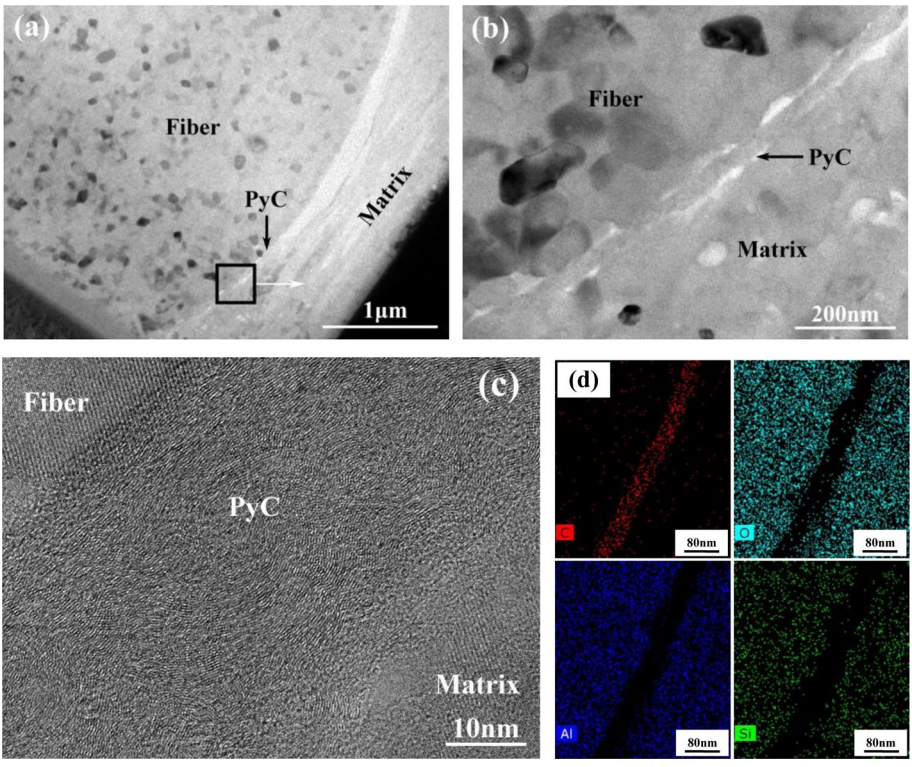

Fig. 10 TEM analysis at the fiber/matrix interface in the composite with a 70 nm-thick PyC interphase fabricated at 1300 °C: (**a-c**) images and (**d**) element mapping

initially increased and then decreased, with the elastic modulus decreasing from 32.7 GPa to 22.2 GPa. The highest value of 100.9 MPa was obtained for the composite with a gap width of 70 nm. As plotted in Fig. 12, the composite with FC interphase displayed similar ductile fracture behaviour as those with PyC interphase. The slope at the beginning of the flexural load–displacement curve and the load fall rate after reaching the maximum decreased gradually as the gap width increased, indicating the reduction of the elastic modulus and the load transfer efficiency. As shown in Fig. 13, the inference could be further proved by increasing length of the pullout fiber as the gap width increased. For the composite with a gap width of 150 nm, the curve showed the slowest

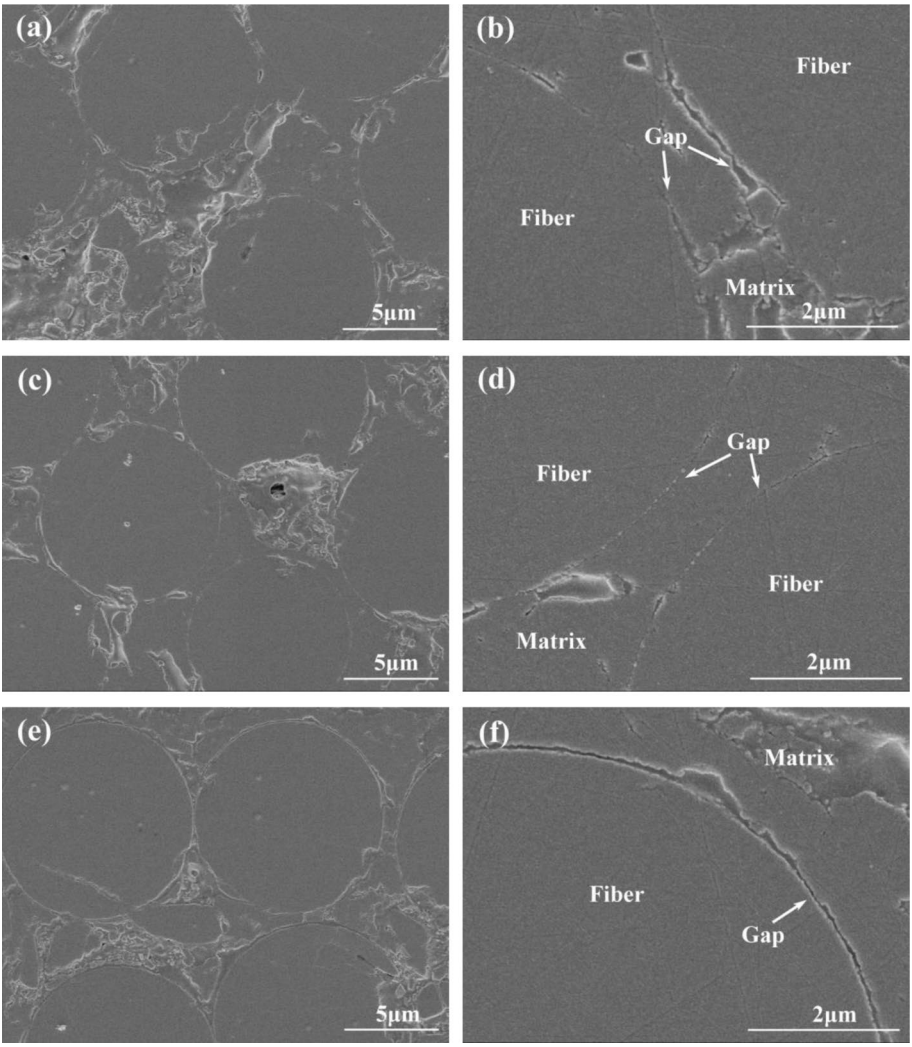

Fig. 11 Cross-section morphology of the composite with different width of FC interphase fabricated at 1300 °C: (**a**)(**b**) 10 nm, (**c**)(**b**) 70 nm and (**e**)(**f**) 150 nm

load fall rate after reaching the maximum with the longest pullout fiber, implying that the lowest flexural strength resulted from the lowest load transfer efficiency.

8 Sintering Temperature Effects on Mechanical Properties of the Composites

The above results showed that the sintering temperature had remarkable effects on the mechanical properties of N440/Al_2O_3-SiO_2 composite. For the composite without interphase, the effect was mainly reflected in different crack propagation behaviour related to porous matrix and interfacial bond strength.

According to the He-Hutchinson model [17], crack deflection will occur when the following condition is satisfied.

$$\Gamma_i/\Gamma_f < G_d/G_p \tag{1}$$

Where Γ_i, Γ_f are the toughness of interface and fiber, and G_d, G_p represent the energy release rate of crack deflection and penetration, respectively. The critical ratio is determined by the elastic mismatch parameter, associated with the modulus of fiber (E_f) and matrix (E_m):

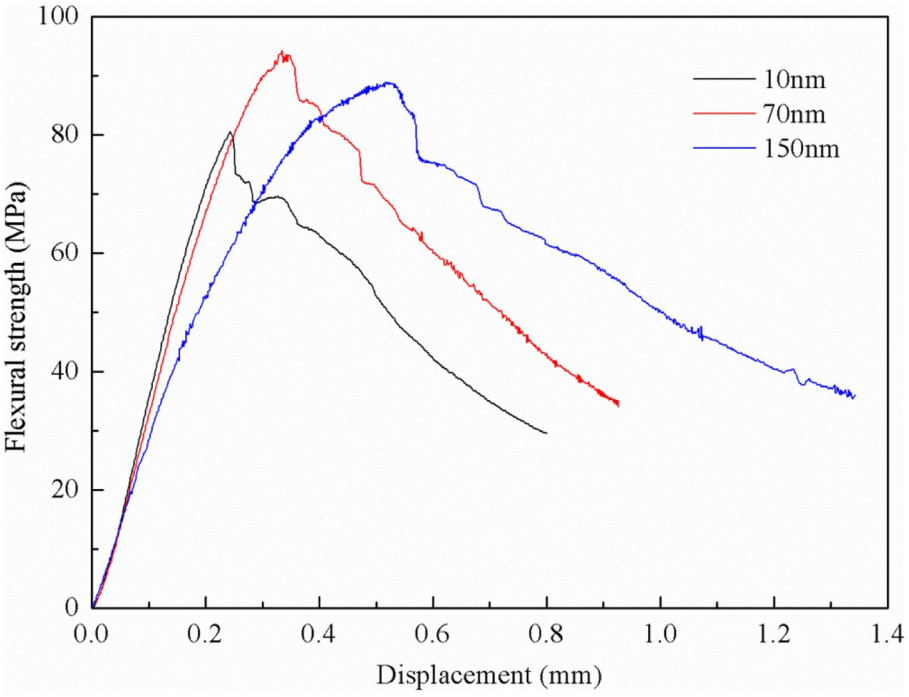

Fig. 12 Typical flexural load–displacement curves of the composite with different width of FC interphase fabricated at 1300 °C

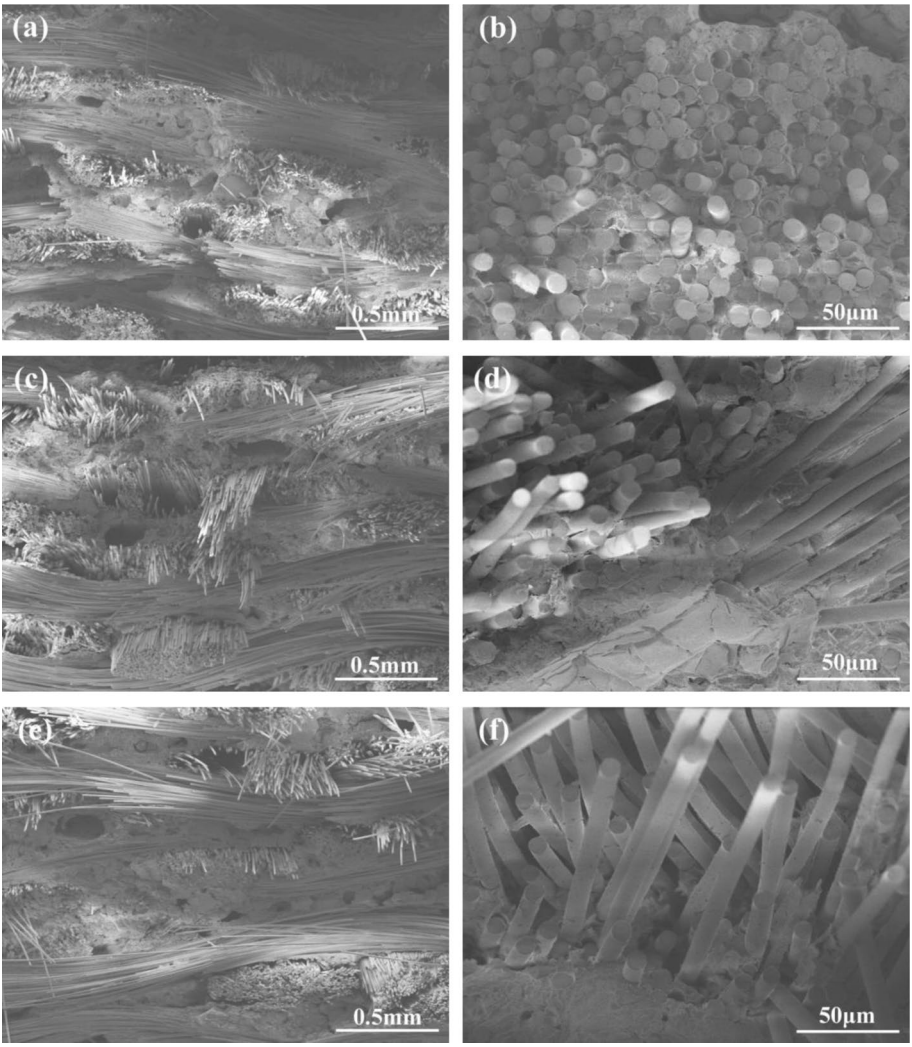

Fig. 13 Fracture surface of the composite with different width of FC interphase fabricated at 1300 °C: (**a**) (**b**) 10 nm, (**c**)(**d**) 70 nm and (**e**)(**f**) 150 nm

$$a \approx \left(E_f - E_m\right)/\left(E_f + E_m\right) \tag{2}$$

As the temperature increased from 1100 °C to 1200 °C, the matrix was strengthened with porosity decreasing from about 35.1% to 30.7%, and elastic modulus and toughness increasing from about 50 GPa to 90 GPa and from about 6 J/m^2 to 9 J/m^2, respectively. As a result, the elastic mismatch parameter decreased and the toughness ratio increased (Fig. 14), and the crack propagation behaviour changed from deflection to penetration [30]. For the composite fabricated at 1100 °C, fiber toughening mechanisms including debonding, bridging and pullout could occur because of crack deflection. Nevertheless, for composites fabricated at 1200 °C and 1300 °C, fiber toughening mechanism could hardly

occur owing to crack penetration. As a result, the composite strength decreased by about 40%, and the fracture behavior changed from ductile to brittle as the sintering temperature increased from 1100 °C to 1200 °C.

For the composite with interphase, the effect of sintering temperature was mainly reflected in the load transfer efficient and in situ fiber strength. The average flexural strength of the composite fabricated at 1300 °C was about 1.31 and 1.46 times higher than that of composites fabricated at 1200 °C and 1400 °C, respectively. The reason for the strength difference was that the lowest load transfer efficient due to the weakest interfacial bond strength was obtained when fabricated at 1200 °C, whereas the lowest in situ fiber strength was induced by high-temperature exposure during the sol–gel process when fabricated at 1400 °C.

9 Interphase Effects on Mechanical Properties of the Composites

Interphase effects on mechanical properties of N440/Al_2O_3-SiO_2 composite were also remarkable. For the composite without interphase, the highest average flexural strength of 90.0 MPa was obtained when the sintering temperature was 1100 °C. However, for the composite with PyC interphase, the highest flexural strength of 116.3 MPa was obtained when the temperature was 1300 °C and the thickness of PyC coatings was 150 nm. In

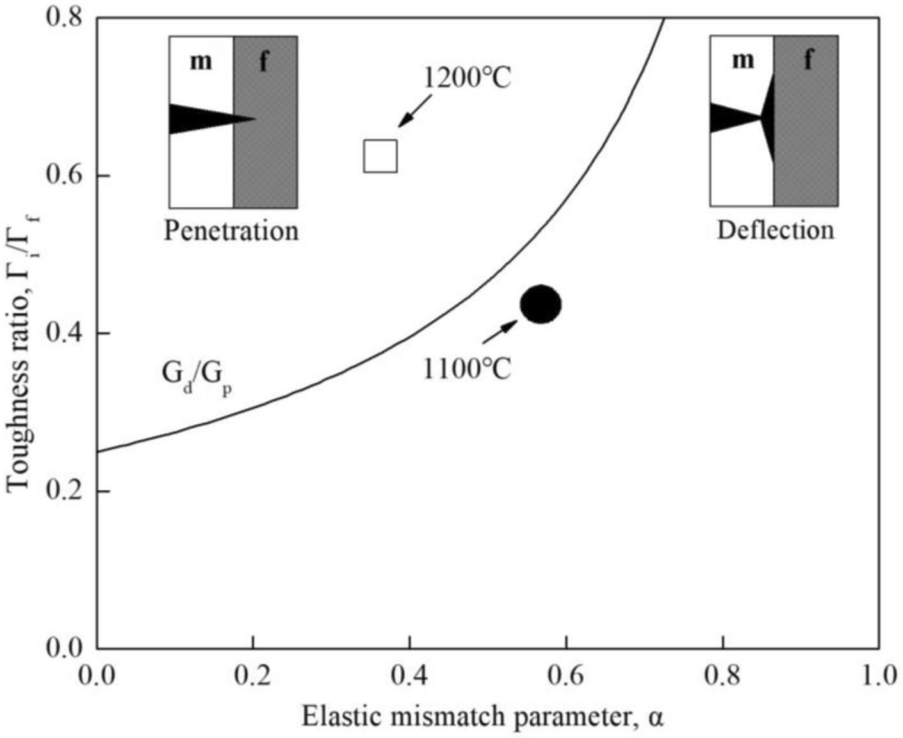

Fig. 14 Effects of sintering temperature on the crack propagation mode. Experimental results were calculated by assuming a toughness ratio $\omega = \Gamma_i/\Gamma_m = 1$ and fiber properties $\Gamma_f = 15$ J/m^2 and $E_f = 190$ GPa

addition, for the composite fabricated at 1300 °C with FC interphase, the highest flexural strength of 100.9 MPa was obtained when the thickness of the FC interphase was 70 nm. After introducing the interphase, on the one hand, the sintering temperature increased by about 200 °C, and a slightly high average flexural strength and equivalent elastic modulus were obtained, which might be meaningful for high-temperature applications of composites considering the combined result of relatively high structural stability of the matrix at elevated temperature and high fiber degradation. On the other hand, the fiber/matrix interfacial properties were improved, and the fracture behaviour of the composite changed from brittle to ductile. Meanwhile, owing to easy preparation through oxidation of PyC interphase and little effects on composition and structure, FC interphase was more suitable to meet the demand of excellent high-temperature oxidation resistance for continuous fiber-reinforced oxide/oxide composites.

To better understand interphase effects on mechanical properties of N440/Al_2O_3-SiO_2 composite, the load transfer was discussed. As illustrated in Fig. 15, for the composite with optimised PyC or FC interphase (70 nm in this work), crack deflection, interface debonding and fiber pullout would occur, and the load could effectively transfer from the matrix to the fiber, thus improving the strength. As the coating thickness or gap width increased (150 nm in this work), further weakened interfacial bond strength was harmful to the load transfer. Consequently, fiber failed with unideal toughening effect, thus causing low strength and stiffness [31, 32].

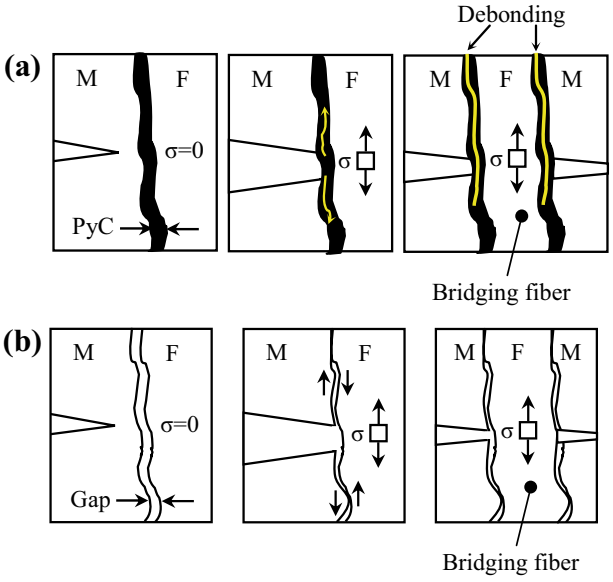

Fig. 15 Schematic digrams of the load transfer in the composite with interphase fabricated at 1300 °C: (**a**) PyC interphase and (**b**) FC interphase

10 Conclusion

Three-dimensional N440/Al_2O_3-SiO_2 composites were fabricated by sol–gel method, and PyC and FC interphase were introduced for interface engineering. The microstructure, mechanical properties and interfacial characteristics of three types of composites were investigated, and the effects of sintering temperature and interphase were discussed. The main conclusions were as follows: The sintering temperature had remarkable effects on the composite strength. For the composite without interphase, the effect was mainly reflected in different crack propagation behaviour related to matrix porosity and interfacial bond strength. For those with interphase, the effect was reflected in the load transfer efficient and in situ fibre strength. The highest average flexural strength (90.0 MPa) was obtained for the composite without interphase fabricated at 1100 °C. The average flexural strength of the composite fabricated at 1300 °C with a 150 nm-thick PyC interphase and a 70 nm-wide FC interphase was 116.3 and 100.9 MPa, respectively. Meanwhile, for the composite fabricated at 1300 °C, the average flexural strength significantly increased after introducing PyC or FC interphase. The main reason for the strength improvement was the effective fibre toughening and matrix/fibre load transfer induced by optimised PyC or FC interphase (70 nm in this work). Further work will focus on interfacial strength analysis of N440/Al_2O_3-SiO_2 composites without and with interphase fabricated at different temperature and systematic investigations on the service properties of optimised composite under high temperature.

Funding This work was financially supported by the National Natural Science Foundation of China (51602347) and the Defense Science and Technology Project Foundation.

References

1. Fan, C.Y., Ma, Q.S., Zeng, K.H.: Bull. Mater. Sci. **41**, 68 (2018)
2. Patel, M., Saurabh, K., Bhanu Prasad, V.V., Subrahmanyam, J.: Bull. Mater. Sci. **35**, 63 (2012)
3. Yang, L.W., Liu, H.T., Jiang, R., Sun, X., Mao, W.G., Cheng, H.F., Molina-Aldareguía, J.M.: J. Eur. Ceram. Soc. **37**, 2991 (2017)
4. Simon, R.A., Danzer, R.: Adv. Eng. Mater. **8**, 1129 (2006)
5. Zhang, W., Ma, Q.S., Dai, K.W., Mao, W.G.: Trans. Nonferrous Met. Soc. China **28**, 2248 (2018)
6. Xiang, Y., Peng, Z.H., Wang, Y., Xing, Z.F., Cao, F.: J. Alloy Compd. **750**, 857 (2018)
7. Tan, H.B., Ma, X.L., Fu, M.X.: Bull. Mater. Sci. **36**, 153 (2013)
8. Hay, R.S., Fair, G.E., Tidball, T.: J. Am. Ceram. Soc. **98**, 1907 (2015)
9. Wamser, T., Scheler, S., Martin, B., Krenkel, W.: J. Eur. Ceram. Soc. **34**, 3827 (2014)
10. Di Salvo, D.T., Sackett, E.E., Johnston, R.E., Thompson, D., Andrews, P., Bache, M.R.: J. Eur. Ceram. Soc. **35**, 4513 (2015)
11. Ruggles-Wrenn, M.B., Lanser, R.L.: Mater. Sci. Eng. A **659**, 270 (2016)
12. Puchas, G., Held, A., Krenkel, W.: Mater. Today: Proceedings **16**, 49 (2019)
13. Yang, Z.M., Yang, J.J.: J. Eur. Ceram. Soc. **40**, 1549 (2020)
14. Venkatesh, R.: Ceram. Int. **28**, 565 (2002)
15. Zok, F.W.: J. Am. Ceram. Soc. **89**, 3309 (2006)
16. Schmücker, M., Grafmüller, A., Schneider, H.: Compos. Part A **34**, 613 (2003)
17. Fujita, H., Jefferson, G., McMeeking, R.M.: J. Am. Ceram. Soc. **87**, 261 (2004)
18. Yang, J.Y., Weaver, J.H., Zok, F.W.: J. Am. Ceram. Soc. **92**, 1087 (2009)
19. Chawla, K.K.: J. Eur. Ceram. Soc. **28**, 447 (2008)
20. Poges, S., Monteleone, C., Petroski, K., Richards, G., Suib, S.L.: Ceram. Int. **43**, 17121 (2017)
21. Wang, Y., Cheng, H.F., Liu, H.T., Wang, J.: Ceram. Int. **39**, 9229 (2013)
22. Wang, Y., Cheng, H.F., Wang, J.: Ceram. Int. **40**, 7269 (2014)

23. Wang, Y., Liu, H.T., Cheng, H.F., Wang, J.: Compos. Part B **75**, 86 (2015)
24. 3M^{TM} Nextel^{TM} Ceramic Fibers and Textiles Technical Reference Guide. Available: https://3M.com/ceramics Accessed on 20 April 2020
25. Oliver, W.C., Pharr, G.M.: J. Mater. Res. **7**, 1564 (1992)
26. Yang, L.W., Wang, J.Y., Liu, H.T., Jiang, R., Cheng, H.F.: Compos. Part B **119**, 79 (2017)
27. Chen, J., Wang, Y., Huang, H., Meng, H.D., Wang, X.L.: Rare Metal. Mater. Eng. **47**, 1281 (2018) (**In Chinese**)
28. Jiang, R., Liu, H.T., Yang, L.W., Sun, X., Cheng, H.F.: Mater. Charact. **138**, 120 (2018)
29. Liu, H.T., Cheng, H.F., Wang, J., Che,.R.C., Tang, G.P., Ma, Q.S.: Mater. Lett. **63**, 2029 (2009)
30. Mattoni, M.A., Yang, J.Y., Levi, C.G., Zok, F.W.: J. Am. Ceram. Soc. **84**, 2594 (2001)
31. Ma, X.K., Yin, X.W., Fan, X.M., Cao, X.Y., Yang, L.W., Sun, X.N., Cheng, L.F.: J. Eur. Ceram. Soc. **39**, 1766 (2019)
32. Weaver, J.H., Yang, J., Zok, F.W.: J. Am. Ceram. Soc. **91**, 4003 (2008)